^{59}Co NMR of Six-Coordinate Cobalt(III) Tetraphenylporphyrin Complexes. 4. The Effect of Phenyl Ortho Substituents on Chemical Shift, Line Width, and Structure

H. Bang, J. O. Edwards,* J. Kim, R. G. Lawler, K. Reynolds, W. J. Ryan, and D. A. Sweigart*

Contribution from the Department of Chemistry, Brown University, Providence, Rhode Island 02912. *Received August 15, 1991*

Abstract: The ^{59}Co NMR spectra have been recorded for a series of sterically congested six-coordinate cobalt(III) porphyrins of the type Co(por)$(RIm)_2^+$, where RIm is imidazole or 1-methylimidazole and por is the dianion of tetramesitylporphyrin (TMP) or tetrakis(2,6-dichlorophenyl)porphyrin (TDCPP). The presence of the ortho chloro or methyl substituents on the meso phenyl groups in the six-coordinate complexes Co(TDCPP)$(RIm)_2^+$ and Co(TMP)$(RIm)_2^+$ has a large effect on the ^{59}Co NMR chemical shifts and line widths when compared to analogous cobalt complexes lacking ortho substituents on the phenyls, e.g., Co(TPP)$(RIm)_2^+$. Extensive studies of solvent effects indicate that the TDCPP and TMP complexes do not experience specific solvation, even with small solvent molecules; the solvent influence is limited to long-range polarity effects. The TPP complexes, on the other hand, exhibit specific, short-range solvation and are able to discriminate among solvents on the basis of size. The X-ray structure of [Co(TDCPP)(1-MeIm)$_2$]BF_4 (**13**) shows that the ortho chloro groups effectively block the space above and below the porphyrin core. The two axial imidazole ligand planes adopt a perpendicular relative orientation with each imidazole plane nearly eclipsing a N_p–Co–N_p bond axis. Additionally, the porphyrin core is substantially ruffled with approximate S_4 symmetry. The distortions produced by the bulky ortho groups in these "hindered" complexes account for the observed solvent dependence of the NMR parameters. Furthermore, strong evidence is presented that the electric field gradient changes sign in going from unhindered to hindered complexes. The structural results provide a ready rationale for this in terms of decreased axial and increased equatorial interaction between the cobalt d-orbitals and the ligand orbitals in the hindered complexes. Compound **13** crystallizes in the monoclinic space group $P2_1/n$ with a = 12.229 (4) Å, b = 21.344 (7) Å, c = 21.227 (7) Å, β = 105.50 (2)°, V = 5339 (3) Å^3, Z = 4, 7622 observed reflections, R = 0.090, and R_w = 0.101.

Introduction

In previous papers[1-3] we demonstrated that ^{59}Co NMR is a useful technique with which to probe in detail the electronic interactions in cobalt(III) porphyrins. Complexes of the type Co(porphyrin)$(RIm)_2^+$, illustrated in Figure 1, have ^{59}Co NMR resonances that are conveniently narrow so that spectral acquisition can be done rather quickly and changes in chemical shift (δ) and in line width ($\omega_{1/2}$) easily measured. As would be expected, δ and $\omega_{1/2}$ depend on substituents at the porphyrin periphery and at the axial imidazole ligands. A substantial dependence on solvent, reflecting general and specific solvation, was also found. The important aspect of this work, from both a practical and theoretical viewpoint, is that the observed changes in chemical shift and line width ($\Delta\delta$ and $\Delta\omega_{1/2}$) can be understood on the basis of a simple molecular orbital model for the metal complex and on the basis of established solvent properties. Briefly, conclusions reached from the previous studies are that (1) porphyrin and imidazole ligands are very close in the spectrochemical series, (2) the cobalt chemical shift is dominated by the temperature-independent paramagnetic contribution, which increases with the inverse of the energy difference, ΔE, between the filled and unfilled d-orbitals on Co, (3) $\omega_{1/2}$ depends on the difference in electron populations between the axial and equatorial Co d-orbitals, (4) both δ and $\omega_{1/2}$ are sensitive to hydrogen bonding from the N–H hydrogen of axial imidazole ligands, and (5) variations of both δ and $\omega_{1/2}$ may be correlated with solvent properties using the multiple-parameter method of Kamlet and Taft.[4] It was also concluded that transmission of electron density from or to substituents on the porphyrin periphery occurs via the porphyrin pπ-orbitals.

These conclusions were derived from results for relatively unhindered complexes having POR, TPP, TPyP or OEP for the porphyrin core in Co(porphyrin)$(RIm)_2^+$. (Figures 1 and 2 illustrate and define the structures and symbols.) Complexes of the *meso*-tetraarylporphyrin type that have substituents at the phenyl positions ortho to the point of attachment to the porphyrin core would be expected to exhibit substantial steric congestion that should influence the axial imidazole ring orientation, the aryl ring orientation, and the extent of solvation of the complex. Given the sensitivity of ^{59}Co NMR to small changes in the electric field near the metal, it was anticipated that these factors and others present in the "hindered" complexes could be investigated by ^{59}Co NMR. Aside from being intrinsically interesting, hindered metalloporphyrin complexes have been extensively studied[5] in oxygenation and, especially, epoxidation and hydroxylation reactions because the reaction intermediates, which are believed to mimic those in protein-mediated processes, have a much greater stability than those formed with unhindered analogues. The origin of this stability enhancement is almost certainly the steric inhibition of bimolecular processes.

In this paper we show that the ortho substituents in TDCPP and TMP complexes cause large changes in the ^{59}Co chemical shifts and line widths and that the dependence of these on solvent differs markedly from that for unhindered analogues. The argument is made that solvation in close proximity to the metal is prevented with the hindered complexes, even with small solvent molecules. This conclusion is supported by the X-ray structure

(1) Hagen, K. I.; Schwab, C. M.; Edwards, J. O.; Sweigart, D. A. *Inorg. Chem.* **1986**, *25*, 978.
(2) Hagen, K. I.; Schwab, C. M.; Edwards, J. O.; Jones, J. G.; Lawler, R. G.; Sweigart, D. A. *J. Am. Chem. Soc.* **1988**, *110*, 7024.
(3) Bang, H.; Cassidei, L.; Danford, H.; Edwards, J. O.; Hagen, K. I.; Krueger, C.; Lachowitz, J.; Schwab, C. M.; Sweigart, D. A.; Zhang, Z. *Magn. Reson. Chem.* **1989**, *27*, 1117.
(4) Kamlet, M. J.; Abboud, J.-L. M.; Abraham, M. H.; Taft, R. W. *J. Org. Chem.* **1983**, *48*, 2877. Kamlet, M. J.; Abboud, J.-L. M.; Taft, R. W. *Prog. Phys. Org. Chem.* **1981**, *13*, 485.
(5) Gunter, M. J.; Turner, P. *Coord. Chem. Rev.* **1991**, *108*, 115. Arasasingham, R. D.; Bruice, T. C. *Inorg. Chem.* **1990**, *29*, 1422. Arasasingham, R. D.; Cornman, C. R.; Balch, A. L. *J. Am. Chem. Soc.* **1989**, *111*, 7800. Traylor, T. G.; Miksztal, A. R. *J. Am. Chem. Soc.* **1989**, *111*, 7443. Groves, J. T.; Stern, M. K. *J. Am. Chem. Soc.* **1988**, *110*, 8628. Groves, J. T.; Watanabe, Y. *J. Am. Chem. Soc.* **1988**, *110*, 8443. Gold, A.; Jayaraj, K.; Doppelt, P.; Weiss, R.; Chottard, G.; Bill, E.; Ding, X.; Trautwein, A. X. *J. Am. Chem. Soc.* **1988**, *110*, 5756. Dicken, C. M.; Woon, T. C.; Bruice, T. C. *J. Am. Chem. Soc.* **1986**, *108*, 1636. Boso, B.; Lang, G.; McMurry, T. J.; Groves, J. T. *J. Chem. Phys.* **1983**, *79*, 1122.

0002-7863/92/1514-2843$03.00/0

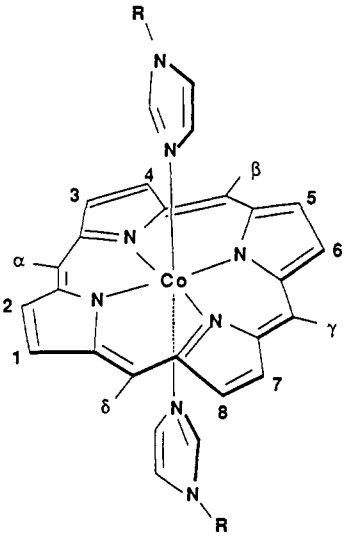

Figure 1. A cobalt(III) porphyrin with axial imidazole ligands. The meso positions are labeled α, β, γ, and δ.

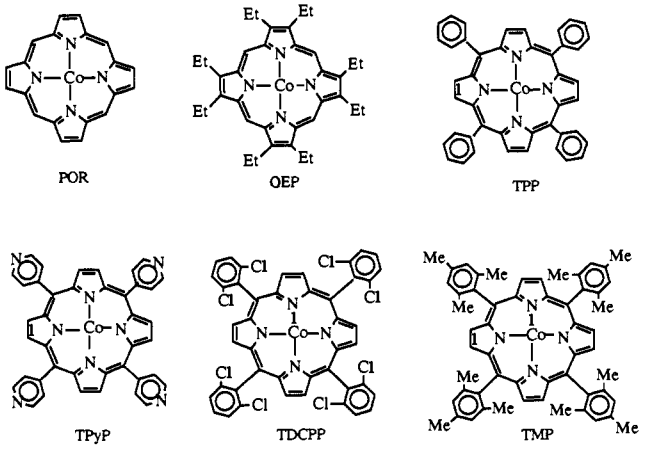

Figure 2. Porphyrins referred to in this study.

of $[Co(TDCPP)(MeIm)_2]BF_4$, which shows that the chloro groups effectively block the space above and below the porphyrin ring, that the meso phenyl rings are locked into nearly perpendicular orientations, and that the axial imidazole planes are perpendicular to each other rather than being parallel as is commonly observed in unhindered metalloporphyrins. The structure also points to a ready explanation for the observed differences in δ and $\omega_{1/2}$ compared to the unhindered cobalt porphyrins.

Experimental Section

General Procedures. The starting compounds, syntheses, solvents, and purifications follow the descriptions in previous papers[1-3] and in the Ph.D. thesis of H. C. Bang (1990). Positive identification of the cobalt complexes was made by ^1H and ^{13}C NMR.

Instrumentation. The ^{59}Co NMR spectra were obtained on a Bruker AM 400 spectrometer (except for a few early experiments on a Bruker WM 250). The NMR samples were filtered into a 10-mm tube fitted with a coaxial 5-mm tube containing the reference (0.10 M $K_3Co(CN)_6$) in lock solvent D_2O. Spectra were recorded with the decoupler off. The temperature was measured with a Doric 410A digital thermometer. A pulse width of 10 μs was used, which corresponds to a pulse angle of 90°; typically 5000 transients were accumulated into 32K data points using an aquisition time of 0.164 s. Line widths at half-height ($\omega_{1/2}$) were computed from peak shapes digitized into typically 800 points per peak. Chemical shifts were normally reproducible to ±2 ppm, with occasional variations up to 4 ppm. The precision of line width measurements was limited primarily by the ability to define the position of half-maximum. The standard deviation of a series of replicate measurements on lines having widths ranging from 200 to 2000 Hz and varying signal/noise ratios was 6%.

Collection and Refinement of X-ray Data. Crystals of $[Co(TDCPP)(MeIm)_2]BF_4$ (**13**) were grown by pentane diffusion into a dichloromethane solution of the complex. A crystal of mean radius 0.19 mm was glued to the end of a glass fiber. Data were collected with a Nicolet R3m diffractometer operating at 20 °C. The unit cell dimensions were calculated from 16 well-centered reflections collected in the range $20° \le 2\theta \le 30°$. The data set was collected by the θ–2θ technique over the range $3.5° \le 2\theta \le 45°$. An empirical absorption correction was made on the basis of azimuthal scans of seven reflections widely separated in reciprocal space.

Analysis of the systematic absences showed the space group to be $P2_1/n$. The structure was solved via direct methods using the SHELXTL 5.1 package.[6] The positions of the cobalt and a number of non-hydrogen atoms were assigned from initial electron density maps, and the positions of the remaining non-hydrogen atoms were located in successive difference Fourier maps. All non-hydrogen atoms of the cation were allowed to refine anisotropically with the weighting scheme $w = 1/[\sigma(F_o)^2 + 0.0004(F_o)^2]$. All hydrogens were placed in theoretical positions, with a C–H bond length of 0.96 Å and a thermal motion parameter equal to 1.2 times that of the attached carbon. The phenyl rings were constrained to regular hexagons (C–C bond length 1.395 Å), and each was refined as a rigid group.

The quality of the refinement was limited by rather large thermal motion of one MeIm ligand (especially the methyl substituent) and disorder in the BF_4^- anion. The MeIm ligand in question, N7–B8–C51–C52–C53–C54, could not be successfully refined by a model placing fractional molecules in two rotational positions. The disorder in the BF_4^- anion could not be satisfactorily modeled. Several large electron density peaks were found arranged around a central peak, identified as B. The group was fixed as a tetrahedron by constraining the B–F distances, and the atoms were refined isotropically. The B atom was refined with a large thermal parameter, which was eventually fixed at 0.500 Å^2. Attempts to refine the BF_4^- as a tetrahedron of varying bond lengths or as several fractional interpenetrating tetrahedra were unsatisfactory; several large peaks of electron density remained unidentified in the vicinity of the anion (but not in contact with the cobalt porphyrin cation). Fractional incorporation of solvent or imidazole was considered, but a successful model could not be found.

Table I. ^{59}Co NMR Data in Acetone at 25 °C

complex number	complex	δ (ppm)	$\omega_{1/2}$ (Hz)
1	$[Co(OEP)(HIm)_2]BF_4$	8821	103
2	$[Co(OEP)(MeIm)_2]BF_4$	8886	190
6	$[Co(TPP)(HIm)_2]BF_4$	8352	343
7	$Co(TPP)(MeIm)_2]BF_4$	8411	533
11	$Co(TPyP)(MeIm)_2]BF_4$	8374	177
12	$[Co(TDCPP)(HIm)_2]BF_4$	8129	120
13	$[Co(TDCPP)(MeIm)_2]BF_4$	8174	231
14	$[Co(TMP)(HIm)_2]BF_4$	7989	1930
15	$[Co(TMP)(MeIm)_2]BF_4$	8008	2180

Results and Discussion

Chemical Shifts. General Comments. The complexes addressed in this study are given a numerical designation in accordance with a previous report.[3] Table I lists the complexes along with ^{59}Co NMR data in acetone. A wide variety of solvents were utilized, and Table II provides a letter designation for each along with the ^{59}Co chemical shifts for seven complexes.

An examination of Table I shows that the hindered complexes **12–15** have much lower chemical shifts than the TPP analogues (**6** and **7**). This change in δ persists in all solvents studied (Table II). Previously, we investigated[2] the dependence of δ on the nature of a substituent (x) at the para position of each phenyl group in $Co(TP_xP)(RIm)_2^+$ complexes. A good correlation was found to exist between δ and the Hammett substituent constants, such that electron-releasing groups increase δ and vice versa. Table III summarizes some of these data, which can be taken as a measure of the sensitivity of δ to electronic effects. As can be seen, *p*-Cl and *p*-Me substituents produce shifts in δ of −1 to −5 ppm and +10 to +15 ppm, respectively. With the assumption that the electronic effects of ortho and para substituents are similar, it is expected that the change in δ for $Co(TDCPP)(RIm)_2^+$ and $Co(TMP)(RIm)_2^+$ should be about −10 and +40 ppm, respectively, compared to $Co(TPP)(RIm)_2^+$. The corresponding observed changes in δ, however, are −250 and −400 ppm. The fact that the observed shifts are an order of magnitude larger, and in the

(6) SHELXTL programs, Nicolet Instrument Co., Madison, WI.

Table II. ^{59}Co Chemical Shifts for Cobalt Porphyrins in Various Solvents at 25 °C[a]

	solvent	δ(6)	δ(7)	δ(11)	δ(12)	δ(13)	δ(14)	δ(15)
A	CF_3CH_2OH	8191	8262	8227		8122		
B	MeOH	8301	8356	8320	8158	8219	8028	8061
C	EtOH	8282	8355	8323	8109	8181	8009	8067
D	*n*-PrOH	8280	8359	8325		8140		8052
E	*n*-BuOH	8313	8381	8332		8130		
F	$HCONMe_2$	8375	8421	8401		8115	7947	7943
G	$PhCH_2OH$	8405	8534	8494		8184		
H	$MeCO_2H$	8360	8414	8352		8226		
I	$MeNO_2$	8343	8367	8318	8119	8185	7959	7970
J	THF	8403	8409	8380		8141		8017
K	Me_2CO	8352	8411	8374	8129	8174	7989	8008
L	Me_2SO	8322	8411	8402	8118	8125	7952	7972
M	MeCOEt	8357	8434	8409		8170		
N	$PhNO_2$	8431	8467	8411	8035	8091	7912	7878
O	MeCN	8347	8369	8320	8155	8210	7990	7999
P	$ClCH_2CH_2Cl$	8358	8396	8378		8117		8010
Q	C_5H_5N	8373	8411	8359		8138		
R	$BrCH_2CH_2Br$	8385	8412	8380		8154		
S	CH_2Cl_2	8389	8450	8420	8095	8186	8012	8066
T	$CHCl_3$	8393	8477	8448	8095	8157	8035	8067
U	*i*-PrOH		*b*	8323		8136		
V	*t*-BuOH		*b*	8314		8096		
W	$HOCH_2CH_2OH$	8277	*b*	8322		8121		
X	$O(CH_2CH_2)_2O$		*b*	*b*		*b*		
Y	$MeCONMe_2$	8377	8471	8456		8167		
Z	PhCN	8412	8435	8394	8060	8076	7913	7881
A′	$MeCO_2CH_2Ph$		8500	*b*		8160		
B′	$MeCO_2Et$	8393	8405	8377		8171		

[a] Chemical shift in parts per million. [b] Too insoluble to obtain NMR spectrum.

Table III. Selected ^{59}Co Chemical Shift and Line Width Data for $[Co(TP_xP)(RIm)_2]BF_4$ Complexes[a]

		series A		series B	
p-X	σ_p[b]	δ (ppm)	$\omega_{1/2}$ (Hz)	δ (ppm)	$\omega_{1/2}$ (Hz)
OMe	−0.27	8459	1580	8316	950
Me	−0.17	8461	1305	8310	770
H	0.00	8447	949	8302	474
Cl	+0.23	8446	892	8297	491
CF_3	+0.55	8438	593	8302	300
CN	+0.63	8410	573	8283	257

[a] Series A refers to $[Co(TP_xP)(MeIm)_2]BF_4$ in CH_2Cl_2 at 25 °C. Series B refers to $[Co(TP_xP)(HIm)_2]BF_4$ in MeOH at 25 °C. [b] Hammett substituent constant.

case of TMP porphyrins of opposite sign, from those predicted points to the steric properties of the ortho substituents, rather than their electronic influence, as the source of the large decrease in δ.

Structure of $[Co(TDCPP)(MeIm)_2]BF_4$. The X-ray structure of complex **13** provides detailed insight into the origin of the steric effects mentioned above. A summary of the diffraction data, atomic coordinates, and bond lengths and angles are given in Tables IV–VII. The atom numbering scheme is provided in Figure 3. Most previous investigations of steric interactions in tetraarylporphyrin complexes focused on bulky axial ligands as the source of the steric congestion. With **13**, on the other hand, the ortho chloro substituents on the meso phenyl rings provide the bulk that, as noted above, leads to different chemical properties in comparison with unhindered analogues. The X-ray study shows that the ortho chloro groups are associated with significant structural changes, as is now discussed.

The porphyrin core in **13** is substantially ruffled, which is probably due to the combined steric requirements of the eight ortho chloro substituents in conjunction with the axial 1-methylimidazole ligands. Of course, crystal packing effects may also play a role, especially when alternative conformations are close in energy for the isolated molecule. Figure 4 gives the displacements of the relevant atoms from the mean plane of the 24-atom core. Overall, the core adopts a nearly S_4 symmetry, with the methine carbon atoms having the largest displacements. The root mean square displacement for the entire core is 0.14 Å, with the largest displacement being 0.23 Å. In contrast, the X-ray structure of

Table IV. Summary of X-ray Diffraction Data for $[Co(TDCPP)(MeIm)_2]BF_4$

complex	$[Co(TDCPP)(MeIm)_2]BF_4$
formula	$C_{50}H_{28}BN_8F_4Cl_8Co$
f_w	1170.2
a, Å	12.229 (4)
b, Å	21.344 (7)
c, Å	21.227 (7)
β, deg	105.50 (2)
V, Å^3	5339 (3)
ρ(calcd), g cm^{-3}	1.46
space group	$P2_1/n$
Z	4
temp, °C	20
radiation	Mo Kα, 0.710 69 Å
μ, cm^{-1}	7.79
2θ limits, deg	3.5–45
observations (total)	7622
unique data	6230 [$I > 1.0\sigma(I)$]
final no. of variables	584
R	0.090
R_w	0.101
GOF	2.83

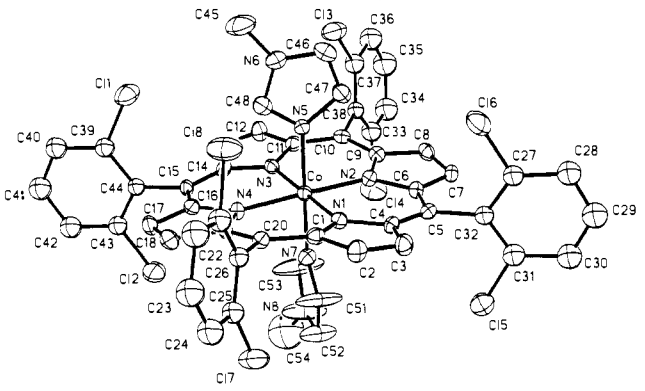

Figure 3. ORTEP diagram of $[Co(TDCPP)(MeIm)_2]BF_4$ (**13**). Probability surfaces are shown at 30%.

$[Co(TPP)(HIm)_2]OAc$ shows that no core atom in this unhindered complex deviates from the mean plane by more than 0.07 Å.[7]

Table V. Atom Coordinates ($\times 10^4$) for $[Co(TDCPP)(MeIm)_2]BF_4$ (13)

atom	x	y	z	atom	x	y	z
Co	1242 (1)	2339 (1)	1011 (1)	C(29)	−5047 (4)	1851 (2)	−782 (2)
N(1)	254 (4)	2774 (2)	242 (2)	C(30)	−4237 (4)	1506 (2)	−989 (2)
N(2)	−42 (4)	1803 (2)	1065 (2)	C(31)	−3085 (4)	1633 (2)	−730 (2)
N(3)	2220 (4)	1921 (2)	1792 (2)	C(32)	−2743 (4)	2105 (2)	−264 (2)
N(4)	2542 (4)	2856 (2)	938 (2)	C(33)	564 (4)	164 (2)	2504 (2)
N(5)	817 (4)	2970 (2)	1560 (2)	C(34)	318 (4)	−236 (2)	2968 (2)
N(6)	772 (5)	3848 (3)	2091 (3)	C(35)	115 (4)	10 (2)	3535 (2)
N(7)	1664 (4)	1715 (3)	452 (2)	C(36)	158 (4)	657 (2)	3638 (2)
N(8)	2356 (10)	878 (3)	113 (4)	C(37)	404 (4)	1056 (2)	3174 (2)
C(1)	515 (5)	3299 (3)	−66 (3)	C(38)	607 (4)	810 (2)	2607 (2)
C(2)	−458 (6)	3488 (3)	−572 (3)	C(39)	5706 (4)	2849 (2)	2663 (2)
C(3)	−1285 (6)	3080 (3)	−581 (3)	C(40)	6870 (4)	2930 (2)	2926 (2)
C(4)	−863 (5)	2642 (3)	−70 (3)	C(41)	7636 (4)	2585 (2)	2683 (2)
C(5)	−1496 (5)	2168 (3)	103 (3)	C(42)	7237 (4)	2158 (2)	2175 (2)
C(6)	−1097 (5)	1775 (3)	635 (3)	C(43)	6072 (4)	2077 (2)	1912 (2)
C(7)	−1774 (5)	1317 (3)	843 (3)	C(44)	5306 (4)	2422 (2)	2156 (2)
C(8)	−1152 (5)	1082 (3)	1410 (3)	C(45)	1094 (8)	4468 (4)	2365 (4)
C(9)	−79 (5)	1377 (3)	1551 (3)	C(46)	−210 (7)	3561 (4)	2051 (4)
C(10)	809 (5)	1247 (3)	2094 (3)	C(47)	−184 (6)	3014 (4)	1730 (4)
C(11)	1889 (5)	1493 (3)	2194 (3)	C(48)	1371 (6)	3486 (4)	1793 (4)
C(12)	2860 (6)	1306 (3)	2716 (3)	C(51)	1478 (10)	1699 (5)	−184 (4)
C(13)	3770 (6)	1605 (3)	2617 (3)	C(52)	1877 (9)	1185 (5)	−399 (4)
C(14)	3378 (5)	1998 (3)	2050 (3)	C(53)	2200 (13)	1206 (5)	616 (5)
C(15)	4051 (5)	2389 (3)	1813 (3)	C(54)	3075 (20)	313 (7)	161 (7)
C(16)	3649 (5)	2801 (3)	1295 (3)	Cl(1)	4783 (2)	3237 (1)	2997 (1)
C(17)	4337 (6)	3249 (3)	1075 (3)	Cl(2)	5598 (2)	1555 (1)	1294 (1)
C(18)	3640 (5)	3593 (3)	611 (3)	Cl(3)	461 (2)	1839 (1)	3313 (1)
C(19)	2525 (5)	3347 (3)	516 (3)	Cl(4)	822 (2)	−144 (1)	1812 (1)
C(20)	1568 (5)	3581 (3)	69 (3)	Cl(5)	−2099 (2)	1226 (1)	−1004 (1)
C(21)	1657 (4)	4755 (2)	−16 (2)	Cl(6)	−3155 (2)	3024 (1)	510 (1)
C(22)	1801 (4)	5299 (2)	−350 (2)	Cl(7)	2017 (2)	3418 (1)	−1261 (1)
C(23)	1998 (4)	5257 (2)	−966 (2)	Cl(8)	1422 (2)	4823 (1)	731 (1)
C(24)	2053 (4)	4671 (2)	−1248 (2)	B	3126 (5)	313 (3)	8033 (3)
C(25)	1909 (4)	4128 (2)	−915 (2)	F(1)	2742 (5)	−215 (3)	7826 (3)
C(26)	1711 (4)	4170 (2)	−298 (2)	F(2)	2910 (5)	697 (3)	7568 (3)
C(27)	−3553 (4)	2450 (2)	−58 (2)	F(3)	2670 (5)	493 (3)	8464 (3)
C(28)	−4705 (4)	2323 (2)	−317 (2)	F(4)	4179 (5)	277 (3)	8270 (3)

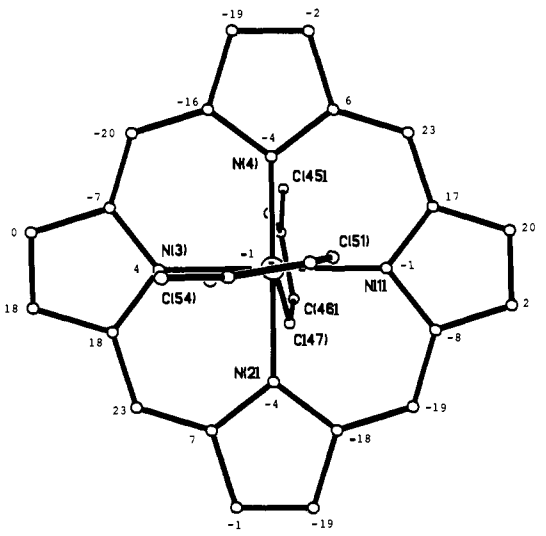

Figure 4. Diagram of $[Co(TDCPP)(MeIm)_2]BF_4$ showing displacements (in units of 0.01 Å) of each atom in the porphyrin core from the mean plane of the 24-atom core. Also shown are the two axial MeIm ligands.

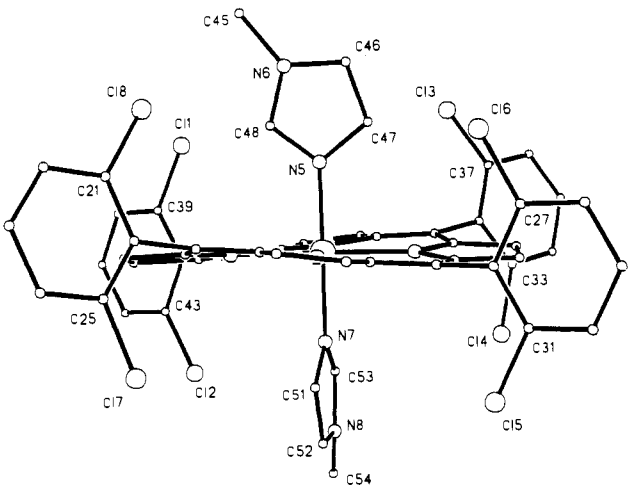

Figure 5. Diagram of $[Co(TDCPP)(MeIm)_2]BF_4$ showing the nearly perpendicular disposition of the meso phenyl rings with respect to the porphyrin core. Also evident is the distortion of the porphyrin core from planarity.

Other comparisons to $[Co(TPP)(HIm)_2]OAc$ (**16**) are informative. The average of the four Co–N_p bond lengths is 1.977 (5) Å for **13** and 1.982 (11) Å for **16**. The axial Co–N_{RIm} bonds are slightly shorter in **16** (1.927 (15) Å) than in **13** (1.942 (6) Å). There are, however, major differences between **13** and **16** in addition to the core distortions mentioned above. The dihedral angles between the phenyl rings and the mean plane of the core in **13** are 81.7°, 82.2°, 86.6°, and 89.6°, showing that the ortho chloro substituents constrain the phenyl groups to be nearly perpendicular to the macrocyclic ring, as illustrated in Figure 5. In **16**, the corresponding angles are 66°, 74°, 86°, and 88°, which are more typical of values found with metalloporphyrins. Another difference between **13** and **16** concerns the relative orientation of the axial imidazole ligand planes. In **16** the planes are parallel (eclipse); in **13** the 1-MeIm axial ligand planes are almost exactly perpendicular (dihedral angle 89.8°).

A useful structural parameter for describing the orientation of planar axial ligands in metalloporphyrins is the dihedral angle (ϕ) between the axial ligand plane and a second plane defined by a M–N_p bond axis and the axial ligand donor atom. If the axial ligand eclipses a N_p–M–N_p bond axis, the value of ϕ is zero;

(7) Lauher, J. W.; Ibers, J. A. *J. Am. Chem. Soc.* **1974**, *96*, 4447.

Table VI. Bond Lengths (Å) for [Co(TDCPP)(MeIm)$_2$]BF$_4$ (13)

bond	length	bond	length	bond	length
Co–N1	1.984 (4)	Co–N2	1.971 (5)	Co–N7	1.941 (6)
Co–N4	1.975 (5)	Co–N5	1.942 (5)	N2–C9	1.384 (8)
N1–C4	1.377 (7)	N1–C1	1.378 (8)	N4–C16	1.369 (7)
N3–C11	1.382 (9)	N3–C14	1.385 (8)	N5–C48	1.318 (9)
N4–C19	1.376 (8)	N5–C47	1.369 (10)	N7–C53	1.269 (12)
N6–C45	1.458 (10)	N6–C48	1.335 (11)	N8–C53	1.332 (14)
N7–C51	1.310 (10)	N8–C52	1.271 (12)	C1–C20	1.381 (9)
N8–C54	1.479 (21)	C1–C2	1.431 (8)	C4–C5	1.381 (10)
C2–C3	1.331 (10)	C3–C4	1.421 (9)	C6–C7	1.426 (10)
C5–C6	1.386 (9)	C5–C32	1.522 (7)	C9–C8	1.414 (9)
C6–N2	1.367 (7)	C8–C7	1.338 (8)	C10–C38	1.504 (8)
C9–C10	1.384 (8)	C10–C11	1.383 (9)	C14–C13	1.439 (9)
C12–C11	1.448 (8)	C13–C12	1.346 (10)	C16–C15	1.389 (8)
C14–C15	1.361 (9)	C15–C44	1.515 (7)	C18–C19	1.424 (9)
C16–C17	1.432 (10)	C17–C18	1.337 (9)	C21–Cl(8)	1.693 (5)
C19–C20	1.387 (8)	C20–C26	1.513 (8)	C31–Cl(5)	1.710 (6)
C25–Cl(7)	1.703 (5)	C27–Cl(6)	1.696 (5)	C39–Cl(1)	1.699 (6)
C33–Cl(4)	1.714 (6)	C37–Cl(3)	1.694 (5)	C47–C46	1.354 (11)
C43–Cl(2)	1.700 (5)	C46–N6	1.330 (11)		
C52–C51	1.328 (16)	Co–N3	1.978 (4)		

Table VII. Bond Angles (deg) for [Co(TDCPP)(MeIm)$_2$]BF$_4$ (13)

atom	angle	atom	angle	atom	angle
N1–Co–N2	90.0 (2)	N1–Co–N3	178.6 (2)	N2–Co–N3	90.1 (2)
N1–Co–N4	90.0 (2)	N2–Co–N4	178.2 (2)	N3–Co–N4	90.0 (2)
N1–Co–N5	88.1 (2)	N2–Co–N5	91.2 (2)	N3–Co–N5	90.4 (2)
N4–Co–N5	90.6 (2)	N1–Co–N7	91.2 (2)	N2–Co–N7	89.1 (2)
N3–Co–N7	90.2 (2)	N4–Co–N7	89.1 (2)	N5–Co–N7	179.3 (2)
Co–N1–C1	127.2 (4)	Co–N1–C4	127.4 (4)	C1–N1–C4	105.4 (5)
N1–C1–C2	109.5 (5)	N1–C1–C20	125.3 (5)	C2–C1–C20	125.2 (6)
C1–C2–C3	107.6 (6)	C2–C3–C4	107.5 (5)	N1–C4–C3	110.0 (6)
N1–C4–C5	125.2 (5)	C3–C4–C5	124.7 (5)	C4–C5–C6	123.9 (5)
C4–C5–C32	119.0 (5)	C6–C5–C32	116.8 (6)	C5–C6–N2	125.6 (6)
C5–C6–C7	124.0 (5)	N2–C6–C7	110.2 (5)	Co–N2–C6	127.6 (4)
Co–N2–C9	127.5 (4)	C6–N2–C9	104.9 (5)	N2–C9–C8	110.4 (5)
N2–C9–C10	125.3 (6)	C8–C9–C10	124.3 (6)	C9–C8–C7	107.2 (6)
C9–C10–C11	123.8 (6)	C9–C10–C38	118.9 (6)	C11–C10–C38	117.3 (5)
Co–N3–C14	127.1 (4)	Co–N3–C11	127.2 (4)	C14–N3–C11	105.8 (5)
N3–C14–C13	109.8 (6)	N3–C14–C15	125.6 (5)	C13–C14–C15	124.6 (6)
C14–C13–C12	107.6 (6)	Co–N4–C16	127.3 (4)	Co–N4–C19	127.2 (4)
C16–N4–C19	105.5 (5)	N4–C16–C17	110.0 (5)	N4–C16–C15	125.5 (6)
C17–C16–C15	124.5 (5)	C16–C17–C18	107.0 (6)	C17–C18–C19	107.5 (6)
N4–C19–C18	110.0 (5)	N4–C19–C20	125.6 (6)	C18–C19–C20	124.4 (6)
C14–C15–C16	124.1 (5)	C14–C15–C44	119.0 (5)	C16–C15–C44	116.7 (5)
C40–C39–Cl(1)	119.5 (2)	C44–C39–Cl(1)	120.4 (2)	C42–C43–Cl(2)	119.5 (2)
C44–C43–Cl(2)	120.5 (2)	C15–C44–C39	120.1 (3)	C15–C44–C43	119.5 (3)
C6–C7–C8	107.3 (5)	C13–C12–C11	107.0 (6)	C10–C11–N3	125.5 (5)
C10–C11–C12	124.6 (6)	N3–C11–C12	109.8 (6)	C34–C33–Cl(4)	119.6 (2)
C38–C33–Cl(4)	120.4 (2)	C36–C37–Cl(3)	119.1 (2)	C38–C37–Cl(3)	120.9 (2)
C10–C38–C33	120.4 (3)	C10–C38–C37	119.5 (3)	C28–C27–Cl(6)	119.3 (2)
C32–C27–Cl(6)	120.7 (2)	C30–C31–Cl(5)	119.7 (2)	C32–C31–Cl(5)	120.2 (2)
C5–C32–C27	119.5 (3)	C5–C32–C31	119.7 (3)	Co–N5–C47	127.5 (4)
Co–N5–C48	127.6 (5)	C47–N5–C48	104.5 (6)	N5–C47–C46	109.5 (7)
C47–C46–N6	106.7 (8)	C46–N6–C45	126.0 (7)	C46–N6–C48	107.6 (6)
C45–N6–C48	126.2 (7)	C1–C20–C19	123.7 (6)	C1–C20–C26	119.0 (5)
C19–C20–C26	117.3 (5)	C22–C21–Cl(8)	118.7 (2)	C26–C21–Cl(8)	121.3 (2)
C24–C25–Cl(7)	119.1 (2)	C26–C25–Cl(7)	120.9 (2)	C20–C26–C21	119.8 (3)
C20–C26–C25	120.2 (3)	N5–C48–N6	111.6 (7)	Co–N7–C53	128.5 (6)
Co–N7–C51	130.3 (6)	C53–N7–C51	101.2 (8)	C52–N8–C53	106.4 (9)
C52–N8–C54	127.5 (10)	C53–N8–C54	125.6 (9)	N8–C52–C51	105.1 (9)
N7–C53–N8	113.8 (8)	N7–C51–C52	113.5 (9)		

this orientation maximizes favorable bonding interactions.[8] Minimization of steric interactions between the porphyrin core and the axial ligand, however, occurs when $\phi = 45°$, i.e., the axial ligand plane bisects the two N_p–M–N_p bond axes. Thus, the interplay of electronic and steric effects may be reflected in the value of ϕ. In **16**, ϕ is 43°, so that the imidazole planes nearly line up with the methine carbon atoms. A similar situation obtains[9] with Fe(TPP)(1-MeIm)N_3 and Fe(TPP)(1,2-Me$_2$Im)N_3, for which the imidazole planes intersect the porphyrin core at ϕ = 42°. In sharp contrast, the MeIm ligand in **13** that is bonded through N5 has $\phi = 11.2°$ and the one bonded through N7 has $\phi = 10.0°$ (see Figure 4). An inspection of the space-filling diagrams in Figure 6 provides an explanation for the reduction in ϕ found in **13**. As can be seen, the ortho phenyl hydrogens in Fe(TPP)(1-MeIm)N_3 are far enough removed from the axial imidazole so that they do not influence its orientation. In **13**, however, the axial imidazoles can avoid unfavorable steric interactions with the ortho chloro groups by nearly eclipsing the Co–N_p bonds (small ϕ). That ϕ is not zero in **13** reflects the interplay of all the factors mentioned above.

(8) Scheidt, W. R.; Chipman, D. M. *J. Am. Chem. Soc.* **1986**, *108*, 1163.
(9) Hallows, W. A.; Ryan, W. J.; Zhang, Y.; Sweigart, D. A. To be published.

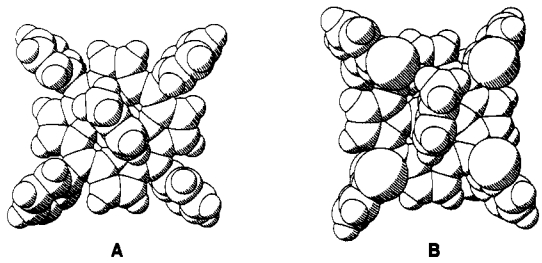

Figure 6. Packing diagram of (A) Fe(TPP)(MeIm)N_3 and (B) [Co(TDCPP)$(MeIm)_2$]BF_4 illustrating the disposition of an axial MeIm ligand with respect to the meso phenyl rings.

The orthogonal disposition of the axial ligands in **13**, the substantial S_4 ruffling of the porphyrin core, the small ϕ angles, and the orthogonal phenyl rings are related to the presence of bulky ortho substituents. It may also be noted (Figure 6) that the space above and below the porphyrin core in **13** is effectively blocked by the chloro groups, so that solvation of Co(TDCPP)$(MeIm)_2^+$ in close proximity to the metal is inhibited, or even prevented. All of these factors give rise to steric and electronic effects that permit a rationalization of the "unusual" ^{59}Co NMR behavior of hindered complexes (vide infra).

A comparison of the structures of **13** and **16** with those of a number of iron(III) porphyrin analogues is useful. Of particular interest are the angle ϕ and the relative orientation (Θ) of the axial imidazole planes. Limiting values of Θ correspond to parallel ($\Theta = 0°$) and perpendicular ($\Theta = 90°$) ligand planes. The structural parameters ϕ and Θ are believed[8,10-15] to significantly influence the chemistry of metalloporphyrins and hemoproteins; the properties affected include spin state, ESR spectra, reduction potentials, and substrate affinities. It is expected[13,15] that imidazole axial ligands would prefer the parallel orientation unless bulky substituents on the porphyrin periphery or on the axial ligands come into play. The unhindered complex [Fe(TPP)$(HIm)_2$]Cl (**17**) crystallizes in several structural forms that depend on the solvent system utilized. One form has a flat TPP core and parallel HIm planes.[16] However, the MeOH solvate of **17** has a S_4 ruffled core (similar to **13**) with $\Theta = 57°$.[17] It would seem, therefore, that alternate structures may not differ much in energy. Other relevant molecules are [Fe(TPP)$(1\text{-MeIm})_2$]ClO_4 (**18**)[18] and [Fe(TPP)$(2\text{-MeIm})_2$]ClO_4 (**19**).[11] Complex **18** has eclipsing 1-MeIm planes ($\Theta = 10°$) while **19** has perpendicular 2-MeIm planes ($\Theta = 89°$; $\phi = 32°$) due to the steric requirements of the 2-Me groups.

Two very recent structures are especially relevant to the results reported herein. [Fe(TMP)$(1\text{-MeIm})_2$]ClO_4 has a flat porphyrin core with parallel axial ligand planes,[15] showing that ortho substituents on the meso phenyl groups do not *guarantee* significant distortions. In contrast, [Fe(TDCPP)$(RIm)_2$]ClO_4 (**20**, RIm = 1-vinylimidazole) possesses a S_4 ruffled core (similar to **13**) with fairly small ϕ angles. In **20**, one of the RIm ligands is disordered with the result that half of the molecules have parallel axial ligand planes ($\Theta = 6°$) and half have roughly perpendicular planes ($\Theta = 76°$); the latter structure was complicated by the presence of a substantial amount of an alternate (impurity) imidazole as one of the axial ligands. In summary, our results indicate that **13** is a very rare example of a porphyrin with perpendicular axial imidazole planes ($\Theta = 90°$) that nearly eclipse the N_p–M–N_p bond axes ($\phi = 10°$ and 11°).

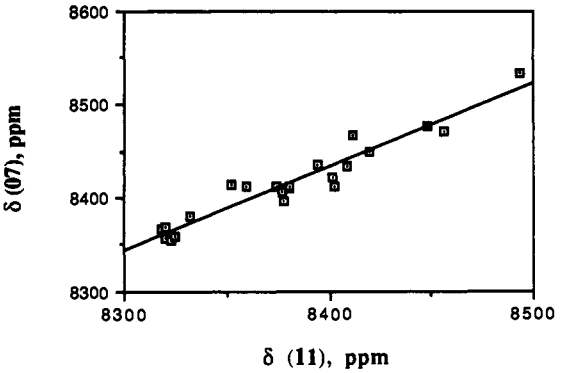

Figure 7. ^{59}Co chemical shifts for the unhindered complex [Co(TPP)$(MeIm)_2$]$^+$ (**7**) versus the unhindered complex [Co(TPyP)$(MeIm)_2$]$^+$ (**11**) in a variety of solvents.

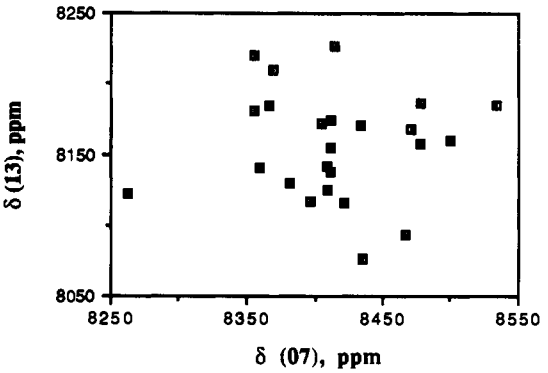

Figure 8. ^{59}Co chemical shifts for the hindered complex [Co(TDCPP)$(MeIm)_2$]$^+$ (**13**) versus the unhindered complex [Co(TPP)$(MeIm)_2$]$^+$ (**7**) in a variety of solvents.

Chemical Shifts. Interpretations. It was previously found[3] that the ^{59}Co chemical shifts of unhindered cobalt porphyrins are strongly positively correlated in different solvents. This is illustrated in Figure 7 for complexes **7** and **11**. Qualitatively, such a correlation is also obtained with the HIm complexes related to **6**. The conclusion is that solvent effects are similar for unhindered complexes, even when, as in the cases of **11** and **6**, the meso and axial substituents may participate in hydrogen bonding. In sharp contrast to this behavior, there is no apparent correlation between the chemical shifts of hindered with unhindered complexes in different solvents. Figure 8 shows a "shotgun" pattern, from which one may conclude that the solvent effects are quite different for hindered and unhindered complexes.

Since the complexes discussed in this paper are charged, it was thought necessary to determine the dependence of the chemical shift on the nature and concentration of the counterion. In methanol, the chemical shift of **12** and **13** remained constant as the concentration of complex varied from 6×10^{-4} to 1×10^{-2} M; more significantly, δ was unaltered (±1 ppm) as the concentration of added KBF_4 spanned the range 0.0010–0.10 M. In dichloromethane, the addition of Bu_4NBr up to 0.32 M caused negligible change in δ for **13**. Estimates of ion pair concentrations using the Fuoss equation[19] indicate that the anticipated increase in ion pairing in dichloromethane with increasing Bu_4NBr concentration is offset by the attendant increase in ionic strength. Our conclusion is that counterion effects on ^{59}Co NMR parameters of porphyrin complexes are small and may be safely ignored in the solvents and at the concentrations studied here.

In a previous study[3] of unhindered complexes, we explored the correlation between chemical shifts and solvent properties using the solvatochromic parameters of Kamlet and Taft.[4] This made possible the identification of both specific, short-range, solvent

(10) Walker, F. A.; Huynh, B. H.; Scheidt, W. R.; Osvath, S. R. *J. Am. Chem. Soc.* **1986**, *108*, 5288.
(11) Scheidt, W. R.; Kirner, J. F.; Hoard, J. L.; Reed, C. A. *J. Am. Chem. Soc.* **1987**, *109*, 1963.
(12) Scheidt, W. R.; Lee, Y. J. *Struct. Bonding (Berlin)* **1987**, *64*, 1.
(13) Inniss, D.; Soltis, S. M.; Strouse, C. E. *J. Am. Chem. Soc.* **1988**, *110*, 5644.
(14) Hatano, K.; Safo, M. K.; Walker, F. A.; Scheidt, W. R. *Inorg. Chem.* **1991**, *30*, 1643.
(15) Safo, M. K.; Gupta, G. P.; Walker, F. A.; Scheidt, W. R. *J. Am. Chem. Soc.* **1991**, *113*, 5497.
(16) Scheidt, W. R.; Osvath, S. R.; Lee, Y. J. *J. Am. Chem. Soc.* **1987**, *109*, 1958.
(17) Collins, D. M.; Countryman, R.; Hoard, J. L. *J. Am. Chem. Soc.* **1972**, *94*, 2066.
(18) Higgins, T. B.; Safo, M. K.; Scheidt, W. R. *Inorg. Chem. Acta* **1990**, *178*, 261.
(19) Fuoss, R. M. *J. Am. Chem. Soc.* **1958**, *80*, 5059.

Table VIII. Solvent Dependence of ^{59}Co Chemical Shifts as Defined by Equation 1[a]

parameter[b]	6	7	11	13	14	15
δ_o (ppm)	8364	8324	8294	8127	8096	8196
s	131	289	299	(51)	(-128)	(-261)
sd	(11)	(-8)	(-24)	-52	(-35)	(-49)
a	(20)	102	79	(50)	(33)	(11)
b	-23	(9)	(-2)	-76	-67	-104
c	-78	-124	-114	(21)	(8)	(42)
no. of solvents	23	22	25	24	11	15
corr coeff	0.87	0.78	0.76	0.73	0.94	0.92

[a] Parameters refer to data obtained at 25 °C. [b] Values in parentheses have a standard error exceeding the magnitude of the parameter and are not statistically significant.

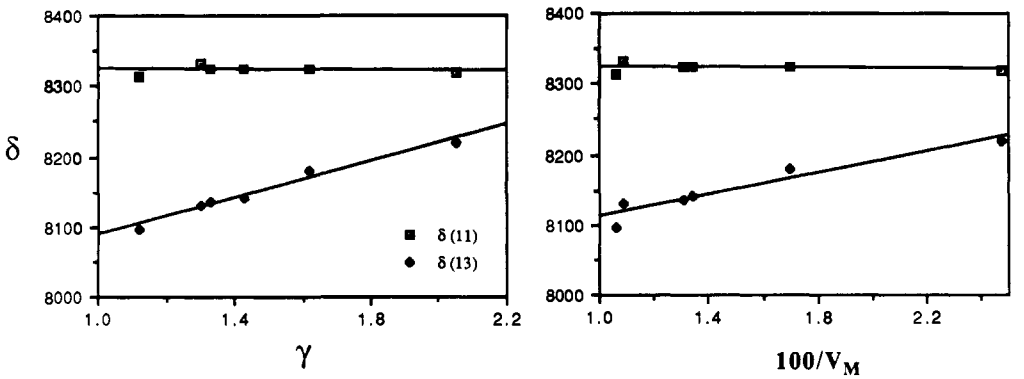

Figure 9. ^{59}Co chemical shifts for $[Co(TPyP)(MeIm)_2]^+$ (**11**) and $[Co(TDCPP)(MeIm)_2]^+$ (**13**) in six aliphatic alcohols (B–E, U, V) versus the solvents' cohesive energy density (γ) and molar volume (V_M).

effects such as hydrogen bonding, as well as general effects due to bulk solvent properties, such as polarity. A similar procedure is reported here for hindered complexes. The relevant relationship is given in eq 1, where the solvent indices are π^* (dipolarity–

$$\delta = \delta_o + s(\pi^* + dp) + a\alpha + b\beta + c\gamma \qquad (1)$$

polarizability), p (discontinuous polarizability correction), α (solvent hydrogen bond donor), β (solvent hydrogen bond acceptor), and γ (internal pressure, solvent cohesive energy density). The indices for the solvents utilized in the present study (Table II) are available elsewhere.[3] Least-squares fitting of chemical shift data for a given complex in a variety of solvents according to eq 1 was performed for six complexes. The results are tabulated in Table VIII.

Examination of the statistically significant coefficients in Table VIII indicates that the chemical shifts of the hindered complexes (**13–15**) are less influenced by solvent change than are the δ values for the unhindered analogues (**6**, **7**, **11**). For the unhindered complexes the variation in δ with solvent is dominated by the terms $s\pi^*$ and $c\gamma$, with a lesser contribution from $a\alpha$; the other terms are either small or have standard errors that exceed the best fit value. In sharp contrast, the chemical shifts for **13–15** do not have a significant dependence on π^*, γ, or α; rather, the only significant index is β, which is unimportant for the unhindered complexes. We ascribe this difference in behavior to the steric effect of the ortho substituents on the meso phenyl groups in **13–15**, which serve to inhibit specific solvation.

The differing solvent effects for the two types of complexes is quantitatively illustrated in Figure 9 for the series of six aliphatic alcohols B–E, U, and V. Shown is the variation of δ(**11**) and δ(**13**) with the cohesive energy density, γ, and the solvent molar volume, V_M. The index γ is a measure of the solvent's self-attachment energy; it increases with functional group polarity and decreases with "dilution" (by simple alkyl groups) of the functional group concentration. As one may expect, γ is inversely related to V_M in a qualitative manner. Figure 9 shows that whereas δ(**11**) changes by only 18 ppm through the series of alcohols, the change in δ for hindered complex **13** is 123 ppm. The surprising insensitivity of the chemical shifts of unhindered complex **11** (or **7**) to alcohol structure (γ or V_M) in spite of the significant value of the coefficient c in eq 1 can be understood as arising from the cancellation of effects due to π^* and α variations that accompany

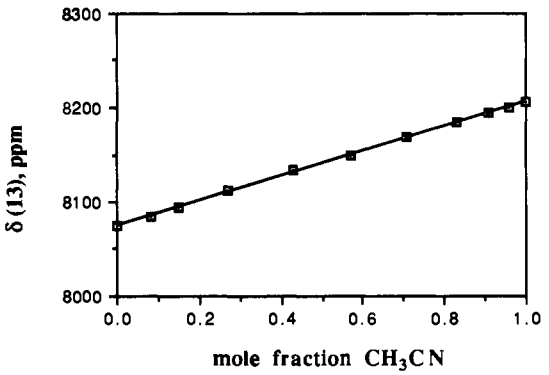

Figure 10. ^{59}Co chemical shifts for $[Co(TDCPP)(MeIm)_2]^+$ (**13**) in mixtures of MeCN and PhCN.

changes in γ and V_M. Paradoxically, the hindered complex **13** has a chemical shift that seems to depend on γ (or V_M) even though the coefficient c in eq 1 is insignificant. In this case, the variation of δ (Figure 9) is due to the decreasing value of $b\beta$ that accompanies increasing V_M (decreasing γ) for the indicated alcohols. We believe, therefore, that the variation of δ(**13**) with γ shown in Figure 9 is not related to solvent size.

Another striking example of the difference between the solvent dependence of δ for the hindered and unhindered complexes is the relative magnitudes of δ in acetonitrile (O) and benzonitrile (Z). Without exception, the unhindered complexes undergo an increase in δ on going from O to Z, whereas the hindered complexes experience an even larger decrease in δ. We interpret this difference to arise from a dominant specific short-range dipolar effect of the small acetonitrile molecule with the unhindered compounds which is opposite in sign from the longer range polarity effects experienced by the hindered complexes. Some indication of the absence of specific solvation of the hindered complexes by acetonitrile is provided by the preferential solvation plot in Figure 10, which shows that δ(**13**) has a strictly linear dependence on the mole fraction of O in mixtures of O and Z. This indicates that neither solvent is preferred, from which it follows that both molecules are excluded from close approach to the metal center. In conjunction with the X-ray results, these observations lead to the general conclusion that the unhinderd complexes experience

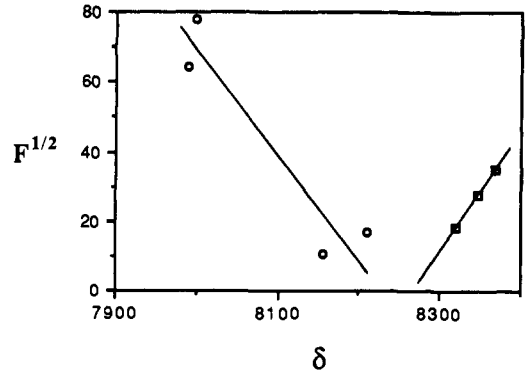

Figure 11. ^{59}Co line width function versus chemical shift for hindered complexes **12–15** (circles) and unhindered complexes **6**, **7**, and **11** (squares). The electric field gradient q is proportional to $\pm F^{1/2}$; the plot shown is essentially equivalent to a graph of q versus δ with the assumption that q has the same sign for all complexes.

specific solvation and are able to discriminate among solvents on the basis of size while specific solvation is minimal for the hindered compounds, even with molecules as small as acetonitrile.

Line Widths. The ^{59}Co NMR line width data for seven cobalt porphyrins in a variety of solvents are given in Table IX. Before considering the influence of solvent on $\omega_{1/2}$, it is useful to examine the implications inherent in the line width data with respect to the electronic properties of the cobalt complexes.

Of the relaxation mechanisms that influence the line widths of six-coordinate low-spin cobalt(III) complexes, quadrupolar coupling is clearly dominant. Equation 2 gives the theoretical expression for quadrupolar relaxation, where $I = {}^7/_2$ for ^{59}Co, ξ

$$\omega_{1/2} = \frac{1}{\pi T_2} = \frac{1}{\pi}\left(\frac{3}{40}\right)\left(\frac{e^2qQ}{\hbar}\right)^2\left(1 + \frac{\xi^2}{3}\right)\left\{\frac{2I+3}{I^2(2I-1)}\right\}\tau_c \qquad (2)$$

is the asymmetry parameter, q is the electric field gradient at the cobalt nucleus, and τ_c is the correlation time for rotational reorientation of the molecule. The near axial symmetry of the cobalt porphyrin complexes means that ξ must be very close to zero. Consequently, the quadrupolar contribution to $\omega_{1/2}$ is determined by two variables, q and τ_c. The latter may be approximated by the Stokes–Einstein model, eq 3, where η is the solvent viscosity

$$\tau_c = (4\pi/3)(a^3\eta/kT) \qquad (3)$$

and a is the hydrodynamic radius of the molecule. For the series of cobalt porphyrins in this study the molecular volume (a^3) is nearly constant. This means that the line width can be written as eq 4, where A and B are constants. The constant A represents

$$\omega_{1/2} = A + Bq^2\eta \qquad (4)$$

nonquadrupolar contributions to the line width and, as indicated previously,[3] has an average value of 81 Hz for cobalt porphyrins. The possible nonquadrupolar line broadening mechanisms have been fully discussed elsewhere.[2] It is convenient for further analysis to eliminate the nonquadrupolar and viscosity dependence of $\omega_{1/2}$ by defining the line width function $F = (\omega_{1/2} - 81)/\eta$, which should depend only on the field gradient q for a series of similar complexes, as in the present study.

In compounds of similar structure, the quantity $F^{1/2}$ should provide a measure of the electric field gradient, q. For small electronic perturbations, e.g., changing a substituent on the meso phenyl rings in the cobalt porphyrins **6–15**, it is expected[20] that q (or $F^{1/2}$) would vary linearly with the chemical shift. Figure 11 shows a plot of $F^{1/2}$ versus δ for the complexes **6–15** in CH_3CN;

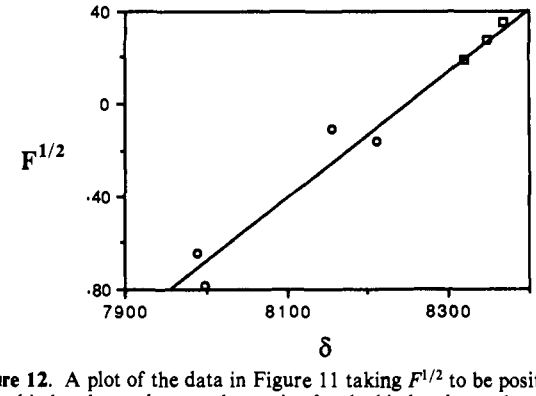

Figure 12. A plot of the data in Figure 11 taking $F^{1/2}$ to be positive for the unhindered complexes and negative for the hindered complexes. The plot shown is essentially equivalent to a graph of q versus δ with the assumption that q changes sign in going from unhindered to hindered complexes.

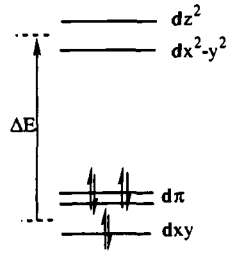

Figure 13. A d-orbital diagram for the unhindered cobalt porphyrin complexes.

similar plots obtain in the other solvents. Since $F^{1/2}$ reflects only the magnitude of q, it was thought possible that the highly nonlinear correlation in Figure 11 signals a change in the sign of q for the hindered complexes compared to the unhindered ones. Indeed, Figure 12 shows that the plot becomes reasonably linear with this assumption.

An examination of the structural details of **13** in conjunction with our earlier work[2] provides a plausible explanation for the change in sign of the electric field gradient with the hindered complexes. Figure 13 gives the d-orbital diagram used[2] to rationalize line width variations with the unhindered cobalt complexes of the type **6**, **7**, **11**, etc. The d_{xy}-orbital does not interact with the porphyrin or imidazole ligands; d_π (d_{xz} and d_{yz}) can interact with π-orbitals on the porphyrin and imidazoles; $d_{x^2-y^2}$ and d_{z^2} can interact with the σ-orbitals on the porphyrin and imidazole nitrogens, respectively. The d_{z^2}-orbital is placed slightly above the $d_{x^2-y^2}$ in accordance with theoretical work;[21] this ordering is also required to explain[2] line width changes. The contribution made by the 3d-orbitals to q may be approximated by eq 5, where

$$q = -{}^4/_7\langle r^{-3}\rangle_d[(N_{z^2} + N_\pi) - (N_{x^2-y^2} + N_{xy})] \qquad (5)$$

$\langle r^{-3}\rangle_d$ is the average value for a single electron in a pure cobalt 3d-orbital and $N_\pi = {}^1/_2(N_{xz} + N_{yz})$ is the average population of the d-orbitals of π-symmetry. With the unhindered complexes we concluded[2] that $[(N_{z^2} + N_\pi) - (N_{x^2-y^2} + N_{xy})] > 0$ and that $N_{z^2} > N_{x^2-y^2}$. In other words, there is greater electron density in the axial d-orbitals than in the equatorial. This arises from the greater σ-interaction between the axial imidazole nitrogens and the cobalt d_{z^2}-orbital. It is important to emphasize, however, that these differences are slight; the chemical shift data clearly show[1] that TPP and RIm ligands are very close in the spectrochemical series. The relatively narrow line widths observed with complexes of the type **6–15** also indicate that q is small, i.e., that the axial and equatorial d-electron densities are nearly the same and that d_{z^2} and $d_{x^2-y^2}$ are very close in energy.

(20) Calderazzo, F.; Lucken, E. A. C.; Williams, D. F. *J. Chem. Soc. A* **1967**, 154. Deverell, C. *Mol. Phys.* **1969**, *16*, 495. Onaka, S.; Miyamoto, T.; Sasaki, Y. *Bull. Chem. Soc. Jpn.* **1971**, *44*, 1851. Bancroft, G. M.; Clark, H. C.; Kidd, R. G.; Rake, A. T.; Spinney, H. G. *Inorg. Chem.* **1973**, *12*, 728. Delville, A.; Detellier, C.; Gerstmans, A.; Laszlo, P. *J. Magn. Reson.* **1981**, *42*, 20. Bryant, R. G. In *NMR of Newly Accessible Nuclei*; Laszlo, P., Ed.; Academic Press: New York, 1983; Vol. 1, p 149.

(21) Antipas, A.; Buchler, J. W.; Gouterman, M.; Smith, P. D. *J. Am. Chem. Soc.* **1978**, *100*, 3015. Antipas, A.; Gouterman, M. *J. Am. Chem. Soc.* **1983**, *105*, 4896. Adar, F.; Gouterman, M.; Aronowitz, S. *J. Phys. Chem.* **1976**, *80*, 2184.

Table IX. ^{59}Co Line Widths for Cobalt Porphyrins in Various Solvents at 25 °C[a]

	solvent	$\omega_{1/2}$(6)	$\omega_{1/2}$(7)	$\omega_{1/2}$(11)	$\omega_{1/2}$(12)	$\omega_{1/2}$(13)	$\omega_{1/2}$(14)	$\omega_{1/2}$(15)
A	CF_3CH_2OH	4123	4449	3781		1194		
B	MeOH	481	956	369	102	195	3300	3635
C	EtOH	835	2007	846	113	399	4259	5744
D	*n*-PrOH	1485	2821	1329		895		9638
E	*n*-BuOH	1302	3987	1693		1139		
F	$HCONMe_2$	275	705	163		597	3065	5491
G	$PhCH_2OH$	3190	3628	1560		1790		
H	$MeCO_2H$	1899	2496	803		556		
I	$MeNO_2$	835	917	353	290	274	3336	4069
J	THF	356	841	353		350		3865
K	Me_2CO	343	533	177	120	231	1930	2180
L	Me_2SO	630	1671	347	217	1514	5235	9114
M	MeCOEt	380	575	201		247		
N	$PhNO_2$	1731	2007	651	1537	1492	10438	11209
O	MeCN	355	522	205	122	182	1573	2279
P	$ClCH_2CH_2Cl$	1780	1817	773		786		6673
Q	C_5H_5N	651	1519	597		776		
R	$BrCH_2CH_2Br$		3309	1427		746		
S	CH_2Cl_2	946	947	400	468	366	3400	3300
T	$CHCl_3$	1425	1283	644	705	594	9304	5859
U	*i*-PrOH		*b*	1546		868		
V	*t*-BuOH		*b*	2740		2224		
W	$HOCH_2CH_2OH$	4899	*b*	3743		2767		
X	$O(CH_2CH_2)_2O$		*b*	*b*				
Y	$MeCONMe_2$	320	787	190		483		
Z	PhCN	1221	1817	543	718	1194	7921	9353
A′	$MeCO_2CH_2Ph$		*b*	*b*		1519		
B′	$MeCO_2Et$		*b*	363		298		

[a] Line width in hertz. [b] Too insoluble to obtain NMR spectrum.

Given that q is small in **6–15**, it is not surprising that a change in the sign of q could accompany the structural changes that occur in the hindered complexes **12–15**. These changes include less meso phenyl ring libration about an orientation perpendicular to the porphyrin ring, increased porphyrin ring distortion, a decrease in the angle ϕ for the axial ligands, and a perpendicular rather than parallel orientation of the axial ligand planes ($\Theta = 90°$). Normally, S_4 ruffling of the porphyrin core of the type present in **13** leads to shorter M–N_p bond distances.[12,15] Comparing **13** and **16**, it may be seen (vide supra) that there is possibly a small decrease in Co–N_p. The lack of a pronounced shortening of Co–N_p may reflect weakened π-interaction that partially compensates for the increased σ-interaction. The expected strengthening of the σ-interaction would raise the equatorial electron density (and $N_{x^2-y^2} + N_{xy}$). A comparison of the Co–N_{RIm} distances in **13** and **16** and in a variety of iron porphyrins[12,15,16] indicates that this bond length increases as the angle ϕ decreases; this is expected from the greater steric interaction with the porphyrin core that occurs at small ϕ angles (vide supra). Such an increase in bond distance implies a weakening of the mixing between d_{z^2} and the axial ligands and an accompanying lowering of axial d-electron density (and $N_{z^2} + N_\pi$). As long as essentially axial symmetry is maintained, the d_{xy}-orbital should remain isolated as the porphyrin structure is changed from unhindered to hindered.

A change in the sign of q implies the inequality $(N_{x^2-y^2} + N_{xy}) > (N_{z^2} + N_\pi)$ for the hindered complexes. A change of electron density in the direction required to satisfy this inequality is supported by the above analysis. In effect, the $d_{x^2-y^2}$- and d_{z^2}-orbitals shown in Figure 13 move closer together or, more likely, invert so that $N_{x^2-y^2} > N_{z^2}$. The observed decrease in chemical shift for the hindered complexes means that ΔE in Figure 13 must increase. This is possible if there is a net raising of the energy of $d_{x^2-y^2}$ and d_{z^2} and/or a lowering of the energy of d_π. The latter could occur if the distortions discussed above lead to decreased interaction of d_π with the ligand π-orbitals or an increased interaction with the ligand π^*-orbitals.

Solvent effects on the line widths are illustrated in Figures 14 and 15, which show that $F^{1/2}$ (or F) for the unhindered complexes **7** and **11** are strongly correlated while $F^{1/2}$ values for **7** (or **11**) are not correlated with $F^{1/2}$ for the hindered complex **13**. This result is not surprising given the conclusion based on chemical shifts (vide supra) that specific solvation occurs with unhindered complexes **6–11**, but is minimal for the hindered analogues **12–15**. Consistent with this view is the much smaller spread of $F^{1/2}$ values

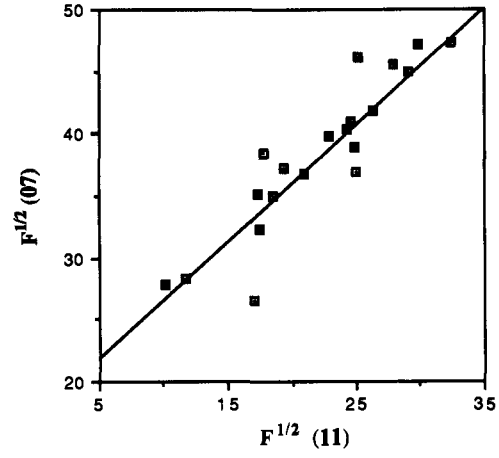

Figure 14. ^{59}Co line width function for the unhindered complex [Co(TPP)(MeIm)$_2$]$^+$ (**7**) versus the unhindered complex [Co(TPyP)(MeIm)$_2$]$^+$ (**11**) in a variety of solvents.

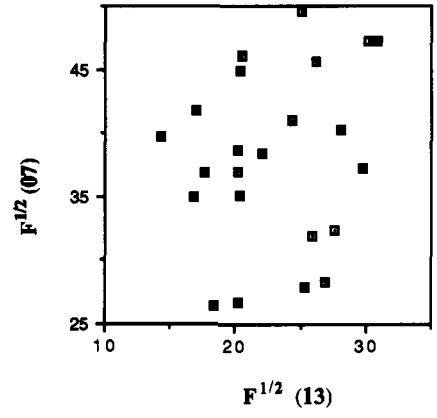

Figure 15. ^{59}Co line width function for the unhindered complex [Co(TPP)(MeIm)$_2$]$^+$ (**7**) versus the hindered complex [Co(TDCPP)(MeIm)$_2$]$^+$ (**13**) in a variety of solvents.

for **12-15** compared to **6-11** as the solvent is changed.

Summary and Conclusions

The presence of ortho chloro or methyl substituents on the meso phenyl groups in the six-coordinate complexes Co(TDCPP)-$(RIm)_2^+$ and Co(TMP)$(RIm)_2^+$ has a large effect on the ^{59}Co NMR chemical shifts and line widths when compared to analogous cobalt complexes lacking ortho substituents on the phenyls, e.g., Co(TPP)$(RIm)_2^+$. Extensive studies of solvent effects indicate that the TDCPP and TMP complexes do not experience specific solvation, even with small solvent molecules; the solvent influence is limited to long-range polarity effects. The TPP complexes, on the other hand, exhibit specific, short-range solvation and are able to discriminate among solvents on the basis of size. The X-ray structure of $[Co(TDCPP)(MeIm)_2]BF_4$ (**13**) shows that the ortho chloro groups effectively block the space above and below the porphyrin core. The two axial imidazole ligand planes adopt a perpendicular relative orientation, with each imidazole plane nearly eclipsing a N_p-Co-N_p bond axis. Additionally, the porphyrin core is substantially ruffled with approximate S_4 symmetry. The distortions associated with the bulky ortho groups in these hindered complexes accounts for the observed solvent dependence of the NMR parameters. Furthermore, strong evidence is presented that the electric field gradient changes sign in going from unhindered to hindered complexes. The structural results provide a ready rationale for this in terms of decreased axial and increased equatorial interaction between the cobalt d-orbitals and the ligand orbitals in the hindered complexes.

Acknowledgment. We gratefully acknowledge the expert experimental assistance of Dr. J. Van Epp and Dr. W. A. Hallows. K.R. was a participant in the NSF Research Experience for Undergraduates program at Brown University in the summer of 1989.

Supplementary Material Available: Hydrogen coordinates (Table SI) and anisotropic thermal parameters (Table SII) for $[Co(TDCPP)(MeIm)_2]BF_4$ (**13**) (3 pages); observed and calculated structure factors (Table SIII) for **13** (42 pages). Ordering information is given on any current masthead page.

Conformational Analysis of a Highly Potent, Constrained Gonadotropin-Releasing Hormone Antagonist. 1. Nuclear Magnetic Resonance

Josep Rizo,[†] Steven C. Koerber,[‡] Rachelle J. Bienstock,[†] Jean Rivier,[‡] Arnold T. Hagler,[§] and Lila M. Gierasch*,[†]

Contribution from the Department of Pharmacology, University of Texas Southwestern Medical Center, 5323 Harry Hines Boulevard, Dallas, Texas 75235-9041, Biosym Technologies, Inc., 10065 Barnes Canyon Road, San Diego, California 92121, and The Clayton Foundation Laboratories for Peptide Biology, The Salk Institute, 10010 North Torrey Pines Road, La Jolla, California 92037. *Received August 19, 1991*

Abstract: Conformational analysis of a cyclic decapeptide analogue of gonadotropin-releasing hormone (GnRH) led to the design of a series of highly potent GnRH antagonists constrained by a bridge between residues 4 and 10 (Struthers, R. S.; et al. *Proteins* **1990**, *8*, 295). We have now used nuclear magnetic resonance (NMR) to study the conformational behavior of one of the most potent of these GnRH antagonists: Ac-Δ^3-Pro1-D-*p*FPhe2-D-Trp3-c(Asp4-Tyr5-D-2Nal6-Leu7-Arg8-Pro9-Dpr10)-NH_2. Our data indicates that a β-hairpin conformation within residues 5-8, stabilized by two transannular hydrogen bonds, is the best defined feature of the molecule. This structure includes a type II' β turn around positions 6 and 7, which has been proposed to be essential for the biological activity of GnRH. Conformational averaging is observed in the Asp4-Dpr10 bridge, most likely favored by the presence of two methylene groups. The linear part of the peptide, the tail formed by residues 1-3, is located above the ring and appears to be somewhat structured: a γ-turn around D-Trp3 is likely to exist, and a type II β turn around residues 1 and 2 could be frequently visited. However, some flexibility and sensitivity to the environment are evident in this region of the molecule. The β-hairpin conformation and the orientation of the tail above the ring correlate with the structure determined for the parent cyclic decapeptide, cyclo(Δ^3-Pro1-D-*p*ClPhe2-D-Trp3-Ser4-Tyr5-D-Trp6-NMeLeu7-Arg8-Pro9-β-Ala10) (Baniak, E. L., II; et al. *Biochemistry* **1987**, *26*, 2642). The conformational model emerging from the NMR data, in combination with our molecular dynamics analysis (see following paper in this issue), suggests additional bridging possibilities to obtain new, more constrained GnRH antagonists.

The last decades have witnessed the discovery of a wide variety of small peptides that modulate diverse biological functions. The definition of the structural requirements for these peptides to play their biological roles is essential to understand their mechanisms of action and to design analogues with potential clinical applications. Despite the variety of biophysical techniques that can be applied to the study of the conformational behavior of these peptides,[1] their analysis is usually hampered by their flexibility and sensitivity to the environment, characteristics that can often be necessary for their function. Perhaps the most sensitive approach to overcome this problem is the design, synthesis, and study of conformationally constrained analogues of the native peptides, which can lead to the definition of the conformational requirements for binding to the corresponding receptor(s), and for agonist or antagonist activity.[2,3]

[†] University of Texas Southwestern Medical Center.
[‡] The Salk Institute.
[§] Biosym Technologies, Inc.

(1) See, for instance *The Peptides: Analysis, Synthesis, Biology*; Udenfriend, S., Meienhofer, J., Hruby, V. J., Eds.; Academic Press: Orlando, FL, 1985; Vol. 7.

0002-7863/92/1514-2852$03.00/0